2D Materials

Controllable, eco-friendly, synthesis of highly crystalline 2D-MoS_2 and clarification of the role of growth-induced strain

To cite this article before publication: Antonios Michail *et al* 2018 *2D Mater.* in press https://doi.org/10.1088/2053-1583/aac610

Controllable, eco-friendly, synthesis of highly crystalline 2D-MoS_2 and clarification of the role of growth-induced strain

Antonios Michail[1,2], John Parthenios[2*], Dimitris Anestopoulos[2], Costas Galiotis[1,3] Meganne Christian[4], Luca Ortolani[4], Vittorio Morandi[4], and Konstantinos Papagelis[1,2,*]

[1]Department of Physics, University of Patras, Patras 26504, Greece

[2]Institute of Chemical Engineering Sciences, Foundation for Research and Technology- Hellas (FORTH/ICE-HT), Patras 26504, Greece

[3]Department of Chemical Engineering, University of Patras, Patras 26504, Greece

[4]Institute for Microelectronics and Microsystems, National Research Council, Bologna 40125, Italy

*Corresponding authors: jparthen@iceht.forth.gr, kpapag@upatras.gr

KEYWORDS

2D materials, Transition metal dichalcogenides, MoS_2, CVD, strain engineering, Raman spectroscopy, Photoluminescence

ABSTRACT

A controlled and eco-friendly, scalable CVD method for the production of single and few layer MoS_2 crystals is proposed. The MoS_2 crystals are fabricated at atmospheric pressure through the reaction of pre-deposited sodium molybdate (Na_2MoO_4) in solution and elemental sulfur at 800 °C, offering the flexibility to achieve two growth regimes -either homogeneously distributed single layer MoS_2 crystals or continuous MoS_2 films- by varying the Na_2MoO_4 solution concentration. In particular, for low precursor concentrations, isolated single layer MoS_2 crystals with controllable mean lateral size were produced. Higher concentrations resulted in continuous single layer films grown in tandem with highly oriented few layer epitaxial domains. The area of the monolayer relative to the few-layer domains can be adjusted. The significant impact on the optical properties of single layer MoS_2 crystals due to the growth induced strain is also examined. The grown monolayer crystals are found to experience ~ 0.3 % biaxial tensile strain relative to the exfoliated ones, while a strain relief of 0.6 % is measured when these CVD crystals are transferred to another plastic substrate. Moreover, in their photoluminescence (PL) spectra, the neutral exciton and negative trion peaks are shifted linearly with biaxial strain. By correlating PL and Raman spectroscopies the deformation potential of the direct optical transition in single layer MoS_2 can be determined.

Introduction

Two-dimensional (2D) transition metal dichalcogenides (TMDCs) possess a unique combination of fundamental solid-state physical phenomena including strong Coulomb exchange, many-body interactions [1, 2], rich excitonic effects [3, 4], large spin-orbit [5, 6]

and spin-valley coupling [3, 7] and thus provide a benchmark to test the physics of 2D systems. Moreover, TMDCs have shown a great potential for diverse applications such as gas sensing [8], actuation [9-11], nanophotonics [12, 13], renewable energy devices (photovoltaics and hydrogen production) [14, 15], electronics [16, 17], quantum manipulation, spintronics and valleytronics [18].

In order to successfully extend the usage of these materials from laboratory to real-life applications, large scale and cost-effective production methods are required. During the past years, several bottom-up [14, 19-28] and top-down [29-35] strategies for the fabrication of atomically thin films have been developed. As has already been proven in the case of graphene, Chemical Vapour Deposition (CVD) method is compatible with industry providing large area high quality material suitable for optoelectronic applications [36]. Extensive attempts to grow atomically thin molybdenum disulphide (MoS_2) through CVD methods have also taken place. In general, the methods developed so far can be divided in one- and two-step processes [37]. In the former method the Mo precursor is introduced in the reactor to act as source for gaseous Mo containing species, while in the latter the Mo precursor is pre-deposited on the substrate prior to thermal treatment [38].

The first and most common single step CVD synthetic route for the fabrication of 2D MoS_2 is the vapor phase reaction between a molybdenum oxide, typically MoO_3 or MoO_2, and elemental sulfur in relatively high temperatures (650 °C - 900 °C) [19, 25, 26, 39-41]. By this approach, triangular single-layer (SL) MoS_2 crystals can be effectively fabricated on the target substrate. Through a continuous refinement of this technique, the quality and the size of the 2D - crystals has increased from a few microns [19] to single crystals with lateral dimensions of hundreds of μm [42, 43]. In some cases, even continuous polycrystalline monolayer films in the mm regime have been obtained, for example, by a space-confined set-up [37, 44].

Continuous films have also been fabricated using $MoCl_5$ instead of MoO_3, and was shown that the thickness of the MoS_2 film depends on the partial pressure of the $MoCl_5$ species, and thus on the amount of the introduced solid $MoCl_5$ in the reactor [45].

Although, one step methods yield relatively large and high-quality crystals, it has been proven difficult to control. More specifically, the nucleation density of MoS_2 crystals on the substrate is inhomogeneous [42] depending strongly on the geometry of the CVD system and, most importantly, on the proximity of the substrate to the MoO_3 source, where sharp spatial concentration gradients occur [43, 46, 47]. Such gradients affect the local Mo:S atomic ratio, which in turn has considerable impact on the growth kinetics of the 2D crystals [46]. Therefore, qualities of the resulting crystals (size, thickness etc.) depend strongly on the geometrical characteristics of the reactor and the utilized substrate, hindering an easy scaling-up of this method [37]. A series of efforts to attain better control of the reaction kinetics in one-step methods, yielding promising results, are the so-called space-confined approaches which have been summarized in a recent review [37].

Two-step methods try to overcome the inhomogeneous nucleation problem by pre-depositing the Mo precursor directly onto the substrate before the reaction with sulfur vapors. Typically, the Mo precursor is a film of elemental Mo, MoO_2, MoO_3 or even a thiomolybdate salt such as $(NH_4)_2\ MoS_4$ [48-50]. In most cases the produced MoS_2 films are predominantly few-layered [48] and may require a low pressure CVD setup in tandem with more complex substrate preparation and treatment which would increase the fabrication costs. It was found that the thickness of the produced MoS_2 film depends on the thickness of the pre-deposited precursor film [50], but so far, obtaining a continuous single-layer (SL) film of MoS_2 has proven to be a non-trivial task.

In this work, a two-step atmospheric pressure CVD method is presented, exhibiting controlled and large area growth of 2D-MoS_2 single and few-layered (FL) crystals through the reaction between sulfur vapors and pre-deposited sodium molybdate (Na_2MoO_4) on a Si/SiO_2 substrate. Sodium molybdate, in contrast to MoO_3 [51], is a non-toxic and environmental friendly water-soluble precursor commonly used as a fertilizer. It is worth noting here that in the past, a hydrothermal reaction between Na_2MoO_4 and KSCN has been utilized to synthesize bulk MoS_2 [52].

It is shown that for low precursor concentrations (< 1.67 mg/mL) the shapes of the fabricated crystals are predominantly SL triangles or three-point stars containing a nucleation point located at their centers. For higher concentrations (>1.67 mg/mL) the crystals tend to merge, forming progressively a continuous SL film with highly oriented and randomly distributed epilayers. Further increase of the precursor concentration results in the coalescence of the epilayers and the production of a bulk crystal. Most importantly, the lateral size and the thickness of the crystals as well as the substrate coverage (monolayer and epilayer domain areas) can be controlled by varying the Na_2MoO_4 precursor concentration providing a more efficient production route. The advantage of the proposed method lies on its flexibility to achieve two different growth regimes depending on the Na_2MoO_4 solution concentration. For low concentrations, isolated and homogeneously distributed monolayer MoS_2 triangles or three-point stars are produced with controllable mean lateral size, while for high concentrations continuous SL films with FL domains are epitaxially formed as was verified from electron diffraction images.

X-ray Photoelectron Spectroscopy (XPS), optical, electron and atomic force microscopies were employed to verify the stoichiometry, crystal quality and morphology of the produced crystals. A variety of crystals were spatially investigated by means of Raman and photoluminescence

(PL) mapping. Based on our previous Raman & PL analysis for SL MoS_2 crystals [53], the level of doping and mechanical strain is quantified and compared with exfoliated samples. A release of the mechanical strain was observed after the deposition of the fabricated CVD crystals onto a polymer substrate. Also, the determination of the mechanical strain imparted to fabricated or transferred SL crystals, enabled the extraction of the direct optical band gap deformation potential for SL-MoS_2 which is in accordance with recent theoretical and experimental studies. The work highlights the importance of the mechanical strain in MoS_2 growth and transfer, while the level of induced strain is adequately high to reliably extract important physical parameters such as deformation potentials and Grüneissen parameters.

Methods

Two-dimensional MoS_2 crystals were synthesized by the reaction of sodium molybdate (Na_2MoO_4) and sulfur vapors in atmospheric pressure and high temperature under inert N_2 atmosphere. In particular, an aqueous solution of $Na_2MoO_4{:}2H_2O$ (Aldrich no. 331058) was spin coated (2000 rpm for 2 min) onto a Si/SiO_2 wafer which was then placed at the centre of the high temperature zone of a quartz tube (1-inch diameter) furnace. A series of samples with different precursor concentrations, namely 0.1 mg/mL, 0.2 mg/mL, 1 mg/mL, 2 mg/mL, 5 mg/mL and 10 mg/mL were prepared. A quartz crucible filled with sulfur powder (Aldrich no. 84683) was placed in the independently controlled low temperature zone, located near the tube end. The tube was purged with nitrogen with a flow of 50 sccm and kept constant during the whole production process. The temperature increased up to 800 °C with a fixed ramp rate of 13 °C/min and held constant at that temperature for 15 minutes. When the main zone's temperature reached 800 °C, the temperature of the sulfur powder increased at a ramp rate of 60°C/min up to 300 °C, well above the sulfur's melting point. Then, the sulfur vapours were carried by the inert nitrogen gas flow towards the reaction zone. After 15 min the reactor was

immediately removed from the furnace to cool down to room temperature. It should be noted that the mass of 2 gr of elemental sulfur was identical for all runs.

Transmission Electron Microscopy (TEM) observations were performed using a FEI Tecnai F20 ST microscope operated at 120 KeV to reduce the radiation damage on the MoS_2 flakes during the observation. The images were captured with a Gatan MSC794 camera. To prepare the samples for TEM observations, the MoS_2 crystals were transferred onto Quantifoil grids using a standard wet transfer procedure (see **Figure S1** in the Supplementary Information) [54]. First, a protective layer of PMMA was spin-coated onto the Si/SiO_2 wafer with MoS_2 crystals, then the wafer was detached by etching the SiO_2 in 1 mol L^{-1} KOH for several hours. The MoS_2-PMMA film was transferred onto a clean wafer and Quantifoil grids were inserted between the film and the wafer. The sample was allowed to dry overnight, then the grids were removed and heated to 200 °C to relax the PMMA, which was then removed in vapours of acetone.

The X-ray photoemission experiments were carried out in an ultra-high vacuum system equipped with a SPECS LHS-10 hemispherical electron analyzer. In all XPS measurements the unmonochromatized Al Kα line at 1486.6 eV and an analyzer pass energy of 36 eV, giving a full width at half maximum (FWHM) of 0.9 eV for the Au $4f_{7/2}$ peak, were used. The XPS core level spectra were deconvoluted by means of mixed Gaussian-Lorentzian peaks after a Shirley background subtraction. Errors are found to be less than 10% (peak areas), while the accuracy of the recording binding energies is ±0.1 eV.

AFM images were taken using a Dimension Icon (Bruker Nano) AFM with ScanAsyst Air probes, or ATESP probes with force constants of 0.4 N/m and 40 N/m, respectively.

Raman and photoluminescence spectra were collected in the backscattering geometry using a Renishaw InVia 2000 spectrometer equipped with a 2400 grooves/mm and 1200 grooves/mm

gratings, providing a spectral resolution of nearly 2.5 cm^{-1} and 7 cm^{-1}, respectively. The spectral accuracy was better than 0.1 cm^{-1} for both gratings (**Figure S2**). For excitation, the 514.5 nm line of an Ar^{+} laser was focused on the sample by means of an ×100 objective lens (NA = 0.85) yielding a beam waist of 470 nm (see supplementary material and **Figure S3)**. In order to avoid unintentional heating of the sample the excitation power was kept below 100 μW in all measurements.

Results and discussion

XPS spectra were collected before and after the reaction of elemental sulfur on top of a Na_2MoO_4 coated substrate and are presented in **Figure 1**. The XPS survey scan (**Figure 1**(a)) revealed that Mo, Si, C and O were present while sulfur was detected only after the treatment. Besides, sodium was detected before treatment and, interestingly, only traces (< 0.5 atom %) were found after the reaction. Before treatment, the existence of a peak doublet (**Figure 1**(b)) located at 232.6 eV and 235.8 eV corresponding to $Mo3d_{5/2}$ and $Mo3d_{3/2}$, respectively, can be assigned to Mo^{6+} chemical state [55]. After treatment, the Mo3d doublet shifted to lower energies at 229.0 eV ($Mo3d_{5/2}$) and 232.1 eV ($Mo3d_{3/2}$), and a new peak appeared at 226.3 eV corresponds to the S2s. Moreover, the S2p peak doublet (**Figure 1**(d)) located at 162.9 eV ($S2p_{1/2}$) and 161.8 eV ($S2p_{3/2}$) is assigned to $S2p_{1/2}$ and $S2p_{3/2}$. The recorded binding energies of Mo3d, S2s and S2p core levels indicate the fabrication of MoS_2 phase on the SiO_2 substrate [56]. Using the peak areas of Mo3d, S2p and the appropriate sensitivity factors (based on Wagner's collection and adjusted to the transmission characteristics of the electron analyzer) the atomic ratio S:Mo is calculated as 1.8 ± 0.2 .

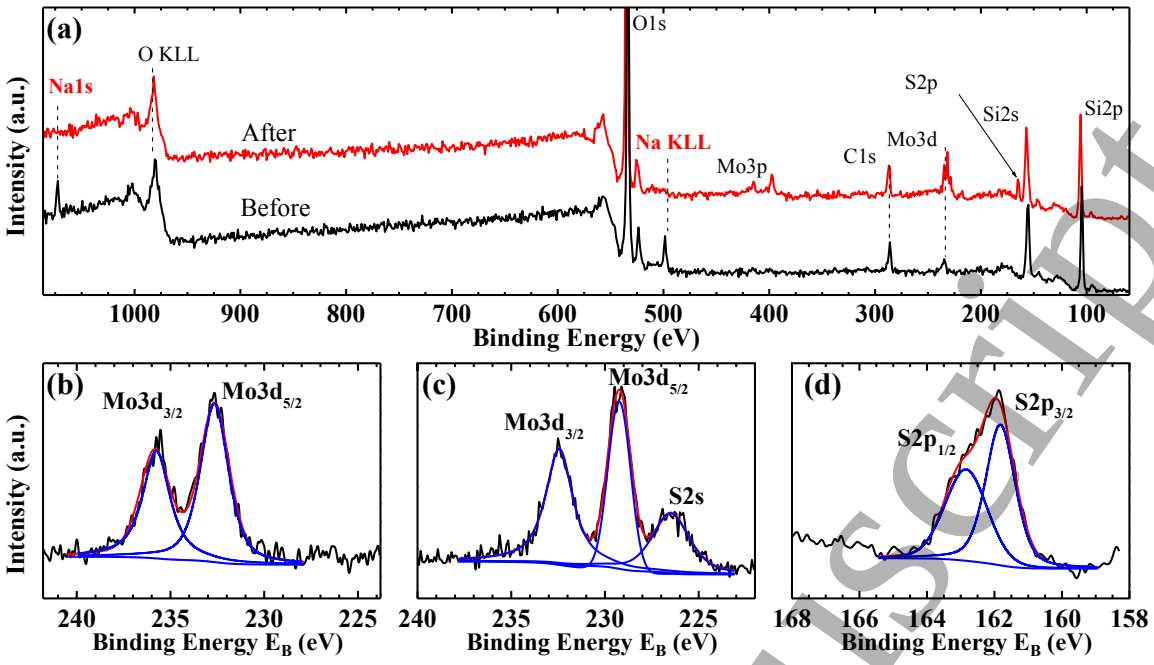

Figure 1 (a) XPS survey scan of a Na_2MoO_4 coated Si/SiO_2 substrate before (black) and after (red) exposure to sulfur vapor. Mo3d and S2s core level peaks of samples before (b) and after (c) heat treatment. (d) $S2p_{1/2}$ and $S2p_{3/2}$ core level peaks of sulfur after treatment.

Figure 2(a)-(d) correspond to optical microscope images of the grown flakes at low levels of Na_2MoO_4 concentration ($\leq$ 2 mg/mL) while **Figure S4** shows the grown continuous films at higher levels of Mo precursor concentration up to 10 mg/mL. For concentrations of Na_2MoO_4 lower than 5 mg/mL, the total area (~ 1.5 x 1.5 cm^2) of the substrate was uniformly covered by three-point star MoS_2 flakes which is a signature of sulfur-rich conditions in the growth region [46, 57]. It has been found that this type of shape is usually developed when the growth rate of the Mo edge is at least three times faster than that of the S edge in the initial hexagonal nuclei [57, 58]. As can be seen in **Figure 2**(a)-(d) and in the inserts, the average crystal size and the nucleation density increase with the Mo precursor solution concentration. At 5 mg/mL the flakes merged and the substrate was almost completely covered, mainly by single- and few-layered MoS_2 as was further verified by Raman and PL spectroscopies (**Figure S5**). It should be noted that at specific locations on the monolayer, MoS_2 epilayers with three-point star or dendritic shapes formed (**Figure S4**(a)). These features are associated with instabilities of the

growth process connected with surface diffusion and self-accelerated localized growth that happens when the corners of the regular shape have access to a higher concentration of Mo precursor [59, 60]. Finally, at 10 mg/mL the substrate was fully covered by bulk crystals of MoS_2 (**Figure S4**(b)).

The morphometric analysis (see supplemental material and **Figure S6**) unveiled a correlation between the Mo precursor concentration and the coverage of the substrate with MoS_2 crystals (monolayers and epilayers). In particular, for concentrations in the range of 0.1 mg/mL to 2 mg/mL the percent coverage of the substrate (*Cov*(%)) increases from 10% to 30%, respectively. While for concentrations higher than 5 mg/mL, *Cov*(%) reaches almost 100% due to the formation of a continuous MoS_2 film (**Figure S4**). The dependence between *Cov(%)* and the Mo precursor solution concentration, *C*, is illustrated in **Figure 2**(e) where the experimental data are fitted by the linear relation: $Cov(\%) = (9.5\ \text{mL/mg})\ C + 10\ \%$. In the supporting information **Table S1** summarizes the substrate's coverage and the ratio of single-layer MoS_2 (or epilayer) domain area to the total MoS_2 area for the precursor concentrations used in this work. As can be verified from **Table S1** and the insets in **Figure S4,** the ratio of the monolayer domain area to that of the epilayer MoS_2 area decreases for concentrations higher than 1.67 mg/mL.

In a large number of three-point star crystals (**Figure 2**(a)-(d)), and at their exact centre, a nucleation point can be clearly identified (blue or white features). As has been proved recently [61], this nucleation centre possesses a core/shell-like structure consisting of an oxysulfide core wrapped in a FL-MoS_2 shell. This fullerene-like structure represents the early stages of the flake growth when the surface is under sulfur deficient atmosphere [61]. It is interesting to note that by increasing the precursor concentration the diameter of the nucleation centre increases

and becomes more pronounced and visible denoting the addition of more MoS_2 layers on the shell structure.

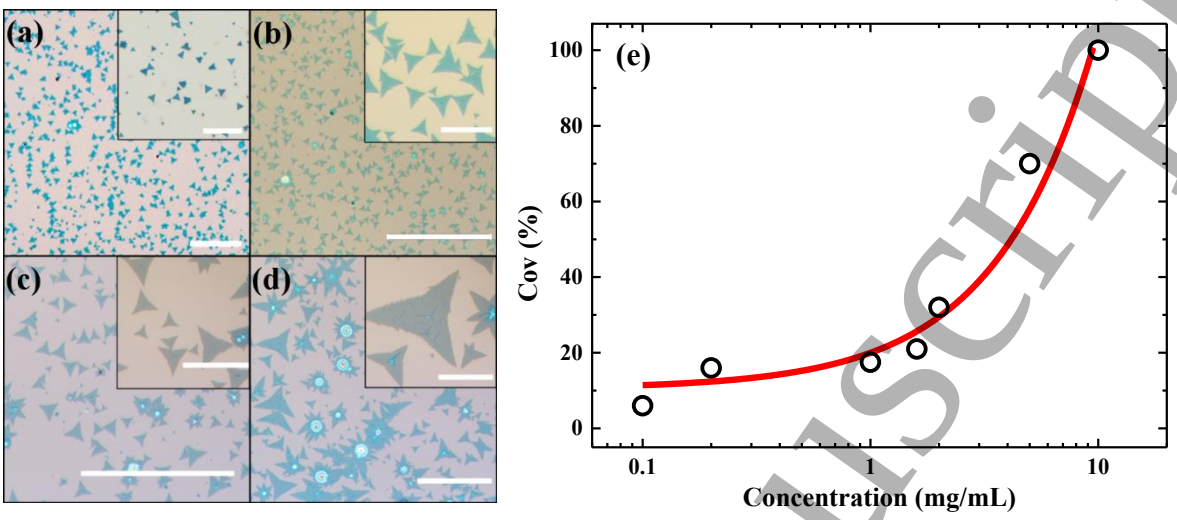

Figure 2 Optical microscope images of samples prepared from Na_2MoO_4 solution with concentrations of (a) 0.1 mg/mL, (b) 0.2 mg/mL, (c) 1 mg/mL, (d) 2 mg/mL. (e) The percent coverage, *Cov*(%), as a function of the Na_2MoO_4 concentration. The concentration axis is logarithmic for clarity. The scale bars in (a) – (d) are 200 μm and in the insets 50 μm.

At low levels of precursor concentration (< 2 mg/mL), the flakes are isolated and randomly oriented on the SiO_2 substrate as shown in **Figure 3**(a). In **Figure 3**(b) an AFM topography image is presented for a monolayer crystal fabricated with a precursor concentration of 1.67 mg/mL. The darker region in the top left corner of the image is the SiO_2 substrate while the rest is a SL-MoS_2 covered with numerous epilayers that grow all over its surface. Their shape has predominantly a three point-star motif, but the most noticeable point is that these secondary formed crystals are all highly oriented along the same direction.

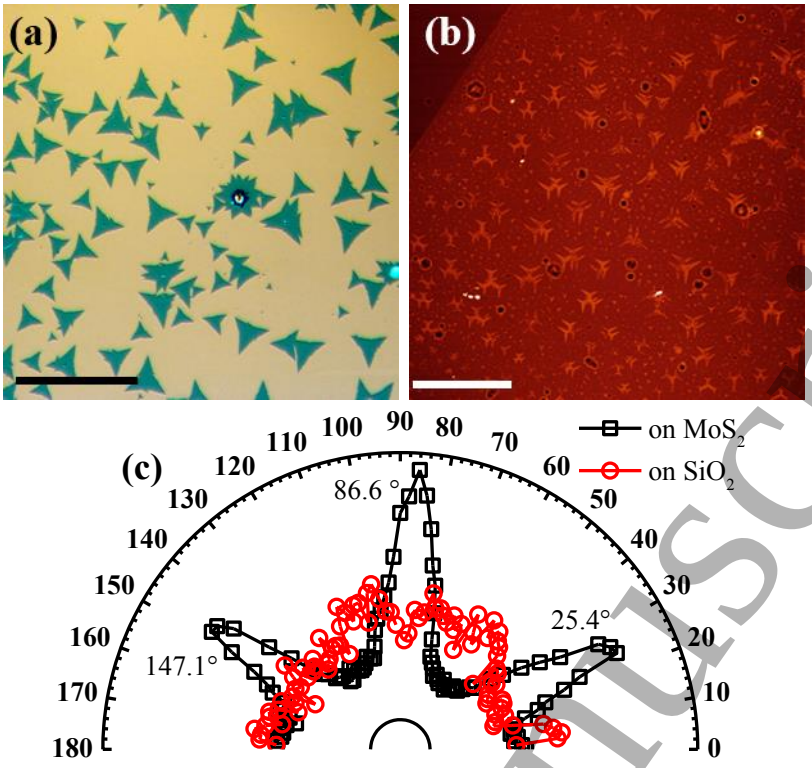

Figure 3 (a) Isolated MoS_2 monolayers as grown on SiO_2 for precursor concentration of 0.2 mg/mL (scale bar 100 μm). (b) AFM topography of monolayer MoS_2 on SiO_2 (1.67 mg/mL). The darker region in the top left corner of the image is the SiO_2 substrate. Epilayer seed crystals have grown on the surface of the monolayer (scale bar 10 μm). (c) Polar directional histogram that shows the dominant directions of the epilayers on MoS_2 monolayer (black squares) and the lack of any preferred orientation of the MoS_2 monolayers on amorphous SiO_2 (red circles).

A more quantitative analysis was conducted through digital image processing in order to investigate the orientation motif of the produced crystals (see supporting information and **Figure S7**). The polar directionality histograms of the epilayers in **Figure 3**(b) are presented as black squares in **Figure 3**(c). The histogram reveals the presence of three preferred directions at 25.4°, 86.6° and 147.2°, which differ by almost 60° reflecting the hexagonal symmetry of the MoS_2 crystals. This phenomenon was found to occur in all MoS_2 monolayers where additional layers (epilayers) grew on top of them (see **Figure S8** for another example**)**. It has been observed that when MoS_2 crystals are grown on single-crystalline substrates, such

as sapphire, they tend to grow with specific crystallographic orientations [62]. As mentioned above, monolayers that grew on SiO_2 were found to be randomly oriented as shown in red circles in **Figure 3**(c)**.** This is an expected outcome since the SiO_2 layer on the top of Si wafers is amorphous. On the other hand, since the secondary layers were grown above the crystalline SL-MoS_2, their consistent crystallographic orientation reflects the high crystallinity of the underlying MoS_2 layer, as was further verified by TEM measurements.

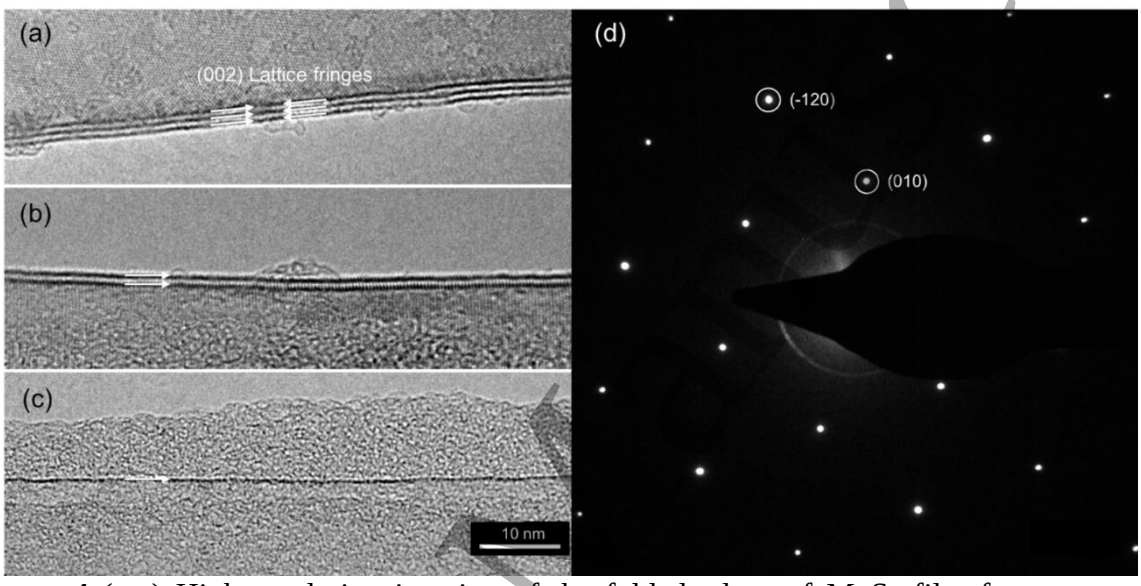

Figure 4 (a-c) High resolution imaging of the folded edges of MoS_2 film from a sample fabricated by 6 mg/mL precursor concentration. The folded edge exposes (002) lattice fringes, spaced by 0.61 nm. (d) Electron diffraction pattern acquired on the internal part of the film in (a), showing hexagonal reflections corresponding to MoS_2 crystal structure along the (002) direction of observation. (-120) and (010) reflections, corresponding respectively to 0.158 nm and 0.273 nm spaced families of crystal planes.

Figure 4(a)-(c) shows high-resolution TEM images of the folded edges from regions of the film with different thicknesses, reflecting the growth of additional layers for 6 mg/mL precursor concentration. The investigation of the (002) lattice fringes at the folds (highlighted by the white arrows) reveals that the local film thickness varies from 1 to 4 layers, and the additional layers grow epitaxially. Electron diffraction analysis of spectra obtained from

different regions of the crystals confirmed the epitaxial growth. **Figure 4**(d) shows an electron diffraction pattern from the internal (not folded) region of the flake shown in **Figure 4**(a). The pattern reveals an individual set of reflections, arranged in a hexagonal system with specific distances compatible with an individual MoS_2 crystal, with layers stacked without rotational defects.

The produced crystals were further investigated by optical spectroscopic techniques such as PL and Raman which have been successfully employed to extract information concerning, among others, the number of layers [63], defects [64], mechanical or thermal strain [65-69], thermal conductivity [70] doping effects [71], stacking order [72] and structural stability [73]. In **Figure 5**(a) an optical microscope image of a supported CVD MoS_2 crystal (Mo precursor concentration of 1.67 mg/mL) is shown, exhibiting two well-defined regions of different optical contrast, assigned as I and II. The PL intensity map of the direct *A* exciton (see below) near 1.80 eV for this crystal is presented in **Figure 5**(b). Two regions, exhibiting high and low PL intensities can be clearly distinguished, corresponding to regions-I and II of **Figure 5**(a). High PL emission in the visible range is a characteristic feature of the direct bandgap present in monolayer MoS_2, while low PL intensity is indicative of an indirect bandgap few-layered (2 to 6 Layers) or even bulk MoS_2 crystal [74]. For freestanding monolayer MoS_2 an enhancement in luminescence efficiency by a factor of 10^2 and 10^4 compared to bilayer and bulk counterparts has been observed [75]. Representative spectra from these regions are depicted in **Figure 5**(c). The individual PL spectra from both regions contain a pronounced peak near 1.80 eV associated with the direct excitonic transitions at the K and K´ points of the Brillouin zone [74]. The valence band of MoS_2 is split in two bands at K/K´ due to the notable spin-orbit coupling arising from the metal d-orbitals [76]. Therefore, two distinct optical transitions assigned as *A* and *B* excitons occur in MoS_2 with the former one located -in freestanding samples- at 1.88 eV and the latter located at 2.05 eV [74, 77]. The PL spectrum from region-II contains another

spectral feature near 1.40 eV, absent from the spectrum of region-I (see inset in **Figure 5**(b)). This peak, assigned as the *I*-exciton, is associated with the indirect gap of few-layered or bulk MoS_2 coming from optical transitions located at the middle point between the high symmetry points K/K´ and Γ in the Brillouin zone [74, 78]. Therefore, these observations verify that region-I corresponds to monolayer MoS_2. Moreover, the exploration of the morphology by means of AFM, of a similar crystal located at the same substrate showed that region-II corresponds essentially to an MoS_2 bilayer (see **Figure S9**). Note that the epilayer coverage of the crystal in **Figure 5** is significantly higher than the average epilayer coverage of crystals fabricated with 1.67 mg/mL precursor concentration (about 11%) as shown in **Table S1**. However, it was chosen for reasons of clarity.

A histogram of the PL peak positions (~1000 spectra) for region I (monolayer) is presented in **Figure 5**(d). The mean value of the PL peak position is 1.78 eV. We found that the PL peak position for many monolayer samples fabricated by the CVD method presented here, is about 1.80 eV, regardless of the Mo precursor concentration (see **Table S2**). This value is about 40 meV redshifted relative to the one reported for exfoliated monolayer MoS_2 on SiO_2 [53, 77]. It is well documented that freestanding MoS_2 is undoped and as a result the A^o neutral exciton (~1.88 eV) dominates the PL emission spectrum. On the other hand, MoS_2 monolayers supported on SiO_2 are *n*-doped and the PL emission is dominated by the recombination of negative trions (A^-) (~ 1.84 eV) [53, 75, 77].

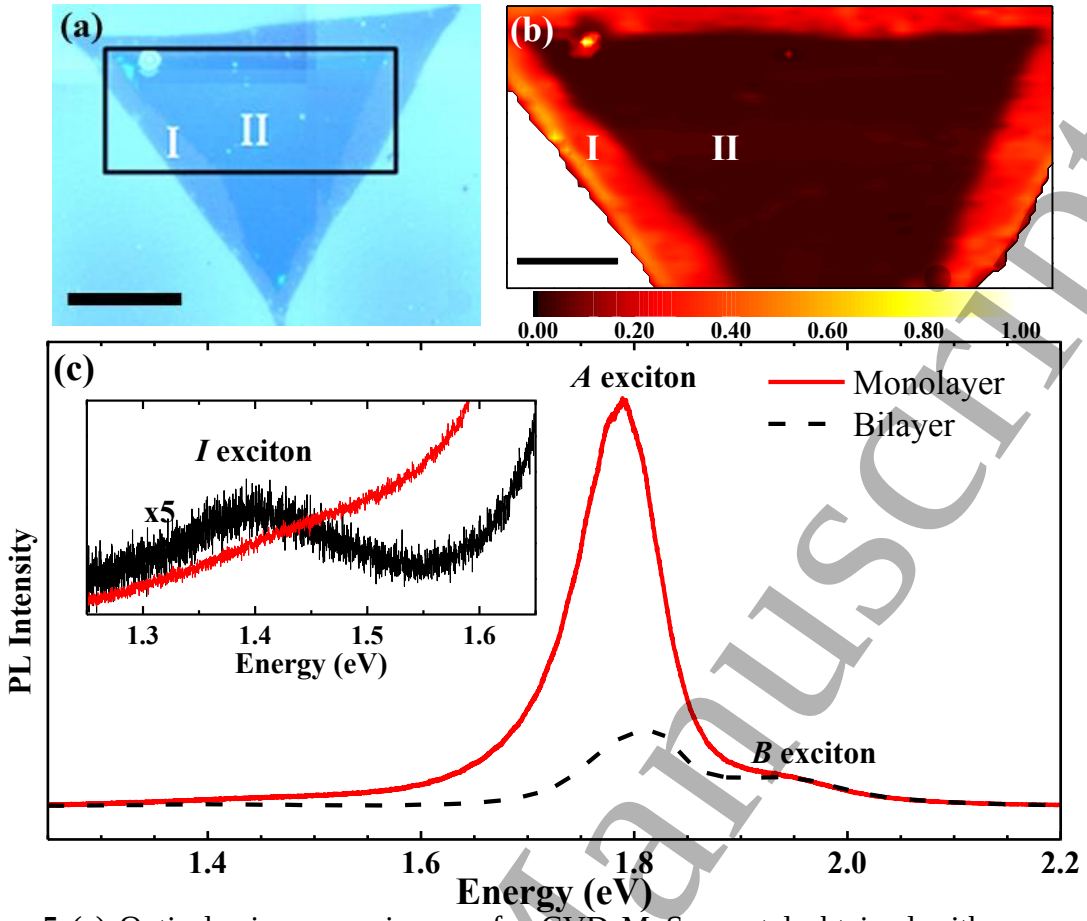

Figure 5 (a) Optical microscope image of a CVD MoS_2 crystal obtained with a precursor concentration of 1.67 mg/mL, where regions I and II of different thickness are denoted. (b) PL Intensity map of the region enclosed by the black rectangle in (a). (c) Representative PL spectra from regions-I (red) and -II (black) where the *A* and *B* exciton emission peaks are visible. The inset shows the spectral region where the *I*-exciton emission peak is visible at 1.4 eV only for region-II. (d) PL peak position histogram from region I. The scale bars in (a) and (b) are 50 μm and 20 μm, respectively.

In **Figure 6**(a), a map of the $\Delta\omega$ value – i.e. the frequency difference between the A_1' and E' Raman modes of SL - MoS_2 – of the above-mentioned MoS_2 crystal is presented (see supporting information). The single- and bilayer - MoS_2 regions exhibit an average $\Delta\omega$ value of 21.8 cm^{-1} and 23.9 cm^{-1}, respectively. The reported $\Delta\omega$ values for exfoliated SL-MoS_2 range between 18.4 cm^{-1} – 19.5 cm^{-1} while, for bilayer- and trilayer - MoS_2 the $\Delta\omega$ values concentrate

close to 21.5 cm^{-1} and 23.5 cm^{-1}, respectively [53, 63]. Comparing the $\Delta\omega$ values of exfoliated MoS_2 with those obtained in the present study for CVD MoS_2 crystals, a significant deviation is noted and will be explained later. Another characteristic example of a CVD MoS_2 crystal exhibiting similar spectral features is presented in **Figure S11**. Note that in that case, the epilayer seeds did not merge and as a result no continuous epilayer formed, yet the spectral response is similar in both cases.

Additional evidence supporting the assignment of regions I and II as a single- and bi-layer MoS_2, respectively, can be given by correlating the Raman scattering intensity of the underlying silicon substrate, I(Si), to the number of MoS_2 layers (N). Due to optical interference effects, the dependence of I(Si) *vs* N is non-trivial (see supporting information). Our calculations show that for $N \leq 3$ and a SiO_2 layer thickness of 90 (300) nm, the I(Si) is found to decrease roughly by 15% (17%) per MoS_2 layer, while, for 20 nm SiO_2 thickness I(Si) is practically constant (**Figure S12**(b)). These results are consistent with the experimental data presented in **Figure S13** and **S14**, were a decrease of I(Si) by (20 ± 4) % and (20 ± 2) % was observed for CVD MoS_2 on 90 nm SiO_2 and for exfoliated MoS_2 on 300 nm SiO_2, respectively. Besides, for CVD MoS_2 crystals grown on 20 nm SiO_2 layer no measurable change in I(Si) was detected **Figure S15**.

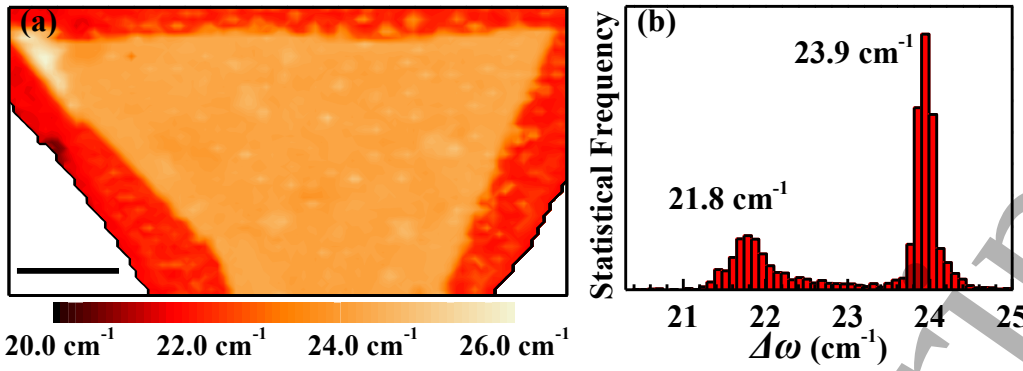

Figure 6 (a) Raman image and (b) histogram of the $\Delta\omega$ value (i.e. the frequency difference between the $A_1'$and E' Raman modes of MoS_2) of the crystal presented in **Figure 5**(a). The scale bar in (a) is 20 μm.

The spectral differences between CVD and exfoliated MoS_2 monolayers reflect the effect of growth conditions and the interaction between the CVD grown crystal and the substrate. This interaction is capable of straining or doping the 2D-crystals with excess charges [79-82]. Moreover, the thermal expansion coefficient (TEC) mismatch between MoS_2 and the Si/SiO_2 substrate can also strain the overlying crystal during the cooling stage [67]. The strain transfer can be influenced due to oxygen dangling bonds present on the SiO_2 surface, which act as anchoring centers for the MoS_2 crystals [83]. It is well documented that mechanical strain can have a measurable impact on both the phonon frequencies [68, 84] as well as the electronic band structure of MoS_2 [66, 85]. This makes Raman and PL spectroscopies suitable non-destructive probes of strain that may be present in 2D-MoS_2 crystals. Additionally, changes in carrier concentration affect both the Raman modes of MoS_2 [71] and its PL response as well [75]. Recently, we have undertaken a systematic study to quantify strain and unintentional doping effects in MoS_2 samples grown or transferred on Si/SiO_2 substrate assuming reasonably that both effects are decoupled from each other at relatively low doping levels (<1%). More specifically, we have shown that it is feasible to quantify local mechanical strain ($\boldsymbol{\varepsilon}$) and doping ($\boldsymbol{n}$) levels in a SL-MoS_2 crystal, by correlating the Pos(A_1') – Pos(E') values obtained in a detailed Raman mapping [53].

In **Figure 7**(a) the Pos(A_1') *vs* Pos(E') plot for a series of representative SL-MoS_2 samples fabricated by CVD or micromechanically exfoliated on different substrates (SiO_2 and PMMA), is presented. Additionally, in the same figure, the strain- charge density (***ε-n***) axes are drawn. Each point in the plot corresponds to the average values for the E' and A_1' phonon mode frequencies, extracted from intensive Raman maps collecting hundreds up to a few thousand spectra. The error bars represent the standard deviation of the corresponding dataset. The data presented graphically in **Figure 7** are summarized in **Table S2** in the supporting information. The shape of the points (square or circle) is indicative of the underlying substrate (SiO_2 or PMMA) while the color (black, red, or blue) represents the sample's fabrication method (CVD, exfoliated or transferred-CVD). It should be noted that the exfoliated onto SiO_2 sample has been considered as a reference for the *ε-n* axes, since, in absence of an undoped and unstrained sample, only strain and carrier concentration differences are meaningful [53].

At first glance, it is evident that all samples experience similar doping levels -0.5 to -1.0x10^{13} electrons/cm^2, except for the SL-MoS_2 crystal exfoliated on SiO_2 substrate which was found to be more *n*-doped. The exfoliated samples, regardless of substrate, experience similar amounts of strain roughly between ±0.05%. The strain and doping levels of the CVD samples are concentrated around 0.3 % and -0.8 x 10^{13} electrons/cm^2, respectively. We found that transferring the CVD samples (blue points) releases the accumulated strain to values in the range of 0.0 to -0.2 %. As a consequence, the $\Delta\omega$ value is decreased from 21.7 cm^{-1} in as fabricated samples to about 19.0 cm^{-1} in transferred CVD samples. These strain and doping differences are also responsible for the aforementioned increased $\Delta\omega$ values of the CVD MoS_2 crystals relative to the exfoliated crystals – 18.4 cm^{-1} and 19.7 cm^{-1} for the SL-MoS_2 exfoliated on SiO_2 and PMMA, respectively. It must be noted that the transferring of a 2D crystal is a sample sensitive, multiple step procedure. As a result, despite that strain relaxation occurred in

all transferred CVD samples, the final states can be different. This is reflected by the presence of the two CVD MoS_2 transferred on PMMMA points (blue circles) in **Figure 7**(a).

More evidence that support the claim that the CVD-MoS_2 crystals are subjected to relatively tensile strain are found in **Figure 7**(b). There, the average PL peak position for the A^o exciton (solid shapes) and A^- trion (open shapes) for the samples (see **Table S2**) presented in **Figure 7**(a) are plotted against the average relative strain that was calculated from the Raman mappings. The data lie roughly on a line with a slope of (-0.16±0.01) eV/% and (-0.14±0.01) eV/% for the A^o and A^- peaks, respectively. This is very close to the calculated value of the deformation potential of SL-MoS_2 for biaxial strain [86, 87] as well as a very recent experimental measurement [85]. Representative PL spectra for each sample type used in this work are presented in **Figure S16**. It must be noted that since exfoliated SL-MoS_2 crystals on SiO_2 are known to be *n*-doped, no measurable neutral exciton peak was found in the PL signal of our corresponding sample. However, both the A^- as well as the A^o components were detected in the PL response of the SL-MoS_2 crystal which was exfoliated onto PMMA. For the two exfoliated samples the negative trion is found to be roughly at 1.83 eV, supporting the conclusion that these particular samples experience similar amounts of mechanical strain, as inferred from Raman spectroscopy. The presence of the neutral exciton in the sample exfoliated on PMMA is another indication that this crystal has a lower electron concentration than the one exfoliated on SiO_2. Again, the same result is concluded from the Raman analysis in **Figure 7**(a).

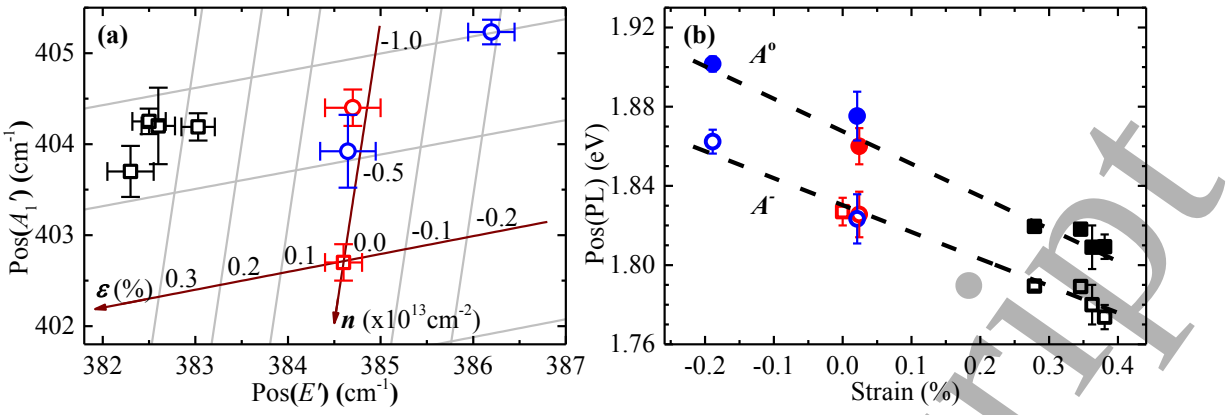

Figure 7 (a) Pos(A_1') vs Pos(E') correlation plot for samples fabricated by different methods and/or supported on different substrates. (b) The average PL peak position of these samples plotted against the relative strain measured from the $\varepsilon - n$ space in (a). The shape of experimental points (square/circle) indicates the substrate (SiO_2/PMMA) and the colour (Black, Red, Blue) indicates the fabrication method (CVD, Exfoliated or transferred CVD).

Conclusions

A novel, controlled and eco-friendly, scalable CVD method for the production of 2D-MoS_2 is developed. Two dimensional MoS_2 crystals are fabricated on Si/SiO_2 substrates through the reaction of Na_2MoO_4 and elemental sulfur at high temperature (800 °C) and atmospheric pressure. Two different growth regimes were observed depending on precursor concentration. Isolated single layer MoS_2 crystals were produced with controllable mean lateral size for concentrations lower than 1.67 mg/mL, while continuous single layers films with few layer domains are epitaxially fabricated for higher concentrations. The method provides homogeneously distributed crystals on the substrate at large scales and control of the monolayer and epilayer areas by varying the Na_2MoO_4 solution concentration. The epilayers were found to be highly oriented, a phenomenon that was attributed to the high crystallinity of the underlying single layer MoS_2.

The CVD crystals exhibit optical spectral differences with respect to their exfoliated counterparts, including higher $\Delta\omega$ values and redshifted PL peak positions. It was made

possible to interpret these peculiarities via a strain – doping ($\boldsymbol{\varepsilon} - \boldsymbol{n}$) correlation plot. The CVD crystals were found to experience tensile strain (~ 0.3 %) relative to the exfoliated ones, while a release of 0.6 % strain was observed when these CVD crystals were transferred to another plastic substrate. Moreover, the neutral exciton and negative trion peak positions of the fabricated crystals varied linearly with biaxial strain in excellent agreement with previous theoretical and experimental studies. Therefore, the correlation of PL and Raman spectroscopies and the relative high level of mechanical stain induced by growth and transfer enabled an indirect measurement of the deformation potential of the direct optical transition of MoS_2 under biaxial strain. The measured deformation potentials were found equal to -0.16 eV/% and -0.14 eV/% for A^o and A^- transitions, respectively, indicating a significant impact of the fabrication method on the optical properties of SL-MoS_2.

Acknowledgements

We thank Dr L. Sygellou, G. Paterakis, for assistance with XPS, AFM measurements, respectively, as well as N. Delikoukos for the production of exfoliated samples. AM, JP, CG, LO, MC, VM and KP acknowledge the financial support of the "Graphene Core 1, GA: 696656–Graphene-based disruptive technologies", which is implemented under the EU-Horizon 2020 Research & Innovation Actions (RIA) and is financially supported by EC-financed parts of the Graphene Flagship and of the European Research Council (ERC Advanced Grant2013) via project no. 321124, 'Tailor Graphene'. This research has been co-financed by the European Union and Greek national funds through the programme "ARISTEIA II: GRAPHENE PHYSICS IN THE TIME DOMAIN AND APPLICATION TO 3D OPTICAL MEMORIES" implemented in the frame of the Operational Program "Education and Lifelong Learning."

References

[1] A. Rustagi and A. F. Kemper (2018) *Theoretical phase diagram for the room-temperature electron–hole liquid in photoexcited quasi-two-dimensional monolayer MoS_2* Nano Letters **18** 455-459

[2] C. H. Lui, A. J. Frenzel, D. V. Pilon, Y. H. Lee, X. Ling, G. M. Akselrod, J. Kong and N. Gedik (2014) *Trion-induced negative photoconductivity in monolayer MoS_2* Physical Review Letters **113** 166801

[3] J. Klein, *et al.* (2018) *Robust valley polarization of helium ion modified atomically thin MoS_2* 2D Materials **5** 011007

[4] J. W. Christopher, B. B. Goldberg and A. K. Swan (2017) *Long tailed trions in monolayer MoS_2: Temperature dependent asymmetry and resulting red-shift of trion photoluminescence spectra* Scientific Reports **7** 14062

[5] Z. Y. Zhu, Y. C. Cheng and U. Schwingenschlögl (2011) *Giant spin-orbit-induced spin splitting in two-dimensional transition-metal dichalcogenide semiconductors* Physical Review B **84** 153402

[6] R. Roldán, M. P. López-Sancho, F. Guinea, E. Cappelluti, J. A. Silva-Guillén and P. Ordejón (2014) *Momentum dependence of spin–orbit interaction effects in single-layer and multi-layer transition metal dichalcogenides* 2D Materials **1** 034003

[7] L. Zhang, K. Gong, J. Chen, L. Liu, Y. Zhu, D. Xiao and H. Guo (2014) *Generation and transport of valley-polarized current in transition-metal dichalcogenides* Physical Review B **90** 195428

[8] H. Li, Z. Yin, Q. He, H. Li, X. Huang, G. Lu, D. W. H. Fam, A. I. Y. Tok, Q. Zhang and H. Zhang (2012) *Fabrication of single- and multilayer MoS_2 film-based field-effect transistors for sensing no at room temperature* Small **8** 63-67

[9] K.-A. N. Duerloo, M. T. Ong and E. J. Reed (2012) *Intrinsic piezoelectricity in two-dimensional materials* The Journal of Physical Chemistry Letters **3** 2871-2876

[10] H. Zhu, Y. Wang, J. Xiao, M. Liu, S. Xiong, Z. J. Wong, Z. Ye, Y. Ye, X. Yin and X. Zhang (2015) *Observation of piezoelectricity in free-standing monolayer MoS_2* Nature Nanotechnology **10** 151-155

[11] W. Wu, *et al.* (2014) *Piezoelectricity of single-atomic-layer MoS_2 for energy conversion and piezotronics* Nature **514** 470-474

[12] Y. Li, J. Zhang, D. Huang, H. Sun, F. Fan, J. Feng, Z. Wang and C. Z. Ning (2017) *Room-temperature continuous-wave lasing from monolayer molybdenum ditelluride integrated with a silicon nanobeam cavity* Nature Nanotechnology **12** 987-992

[13] O. Lopez-Sanchez, D. Lembke, M. Kayci, A. Radenovic and A. Kis (2013) *Ultrasensitive photodetectors based on monolayer MoS_2* Nature Nanotechnology **8** 497-501

[14] A. Antonelou, G. Syrrokostas, L. Sygellou, G. Leftheriotis, V. Dracopoulos and N. Yannopoulos, Spyros (2016) *Facile, substrate-scale growth of mono- and few-layer homogeneous MoS_2 films on Mo foils with enhanced catalytic activity as counter electrodes in DSSCs* Nanotechnology **27** 045404

[15] Y.-H. Chang, C.-T. Lin, T.-Y. Chen, C.-L. Hsu, Y.-H. Lee, W. Zhang, K.-H. Wei and L.-J. Li (2013) *Highly efficient electrocatalytic hydrogen production by MoS_x grown on graphene-protected 3d Ni foams* Advanced Materials **25** 756-760

[16] B. Radisavljevic, A. Radenovic, J. Brivio, V. Giacometti and A. Kis (2011) *Single-layer MoS_2 transistors* Nature Nanotechnology **6** 147-150

[17] S. Wachter, D. K. Polyushkin, O. Bethge and T. Mueller (2017) *A microprocessor based on a two-dimensional semiconductor* Nature Communications **8** 14948

[18] Z. Ye, D. Sun and T. F. Heinz (2016) *Optical manipulation of valley pseudospin* Nature Physics **13** 26

[19] Y.-H. Lee, *et al.* (2012) *Synthesis of large-area MoS_2 atomic layers with chemical vapor deposition* Advanced Materials **24** 2320-2325

[20] T. Payam, *et al.* (2016) *Growth mechanism of largescale MoS_2 monolayer by sulfurization of MoO_3 film* Materials Research Express **3** 075009

[21] S. J. Yun, *et al.* (2015) *Synthesis of centimeter-scale monolayer tungsten disulfide film on gold foils* ACS Nano **9** 5510-5519

[22] Y. Kobayashi, S. Sasaki, S. Mori, H. Hibino, Z. Liu, K. Watanabe, T. Taniguchi, K. Suenaga, Y. Maniwa and Y. Miyata (2015) *Growth and optical properties of high-quality monolayer WS_2 on graphite* ACS Nano **9** 4056-4063

[23] Y. Jung, J. Shen, Y. Liu, J. M. Woods, Y. Sun and J. J. Cha (2014) *Metal seed layer thickness-induced transition from vertical to horizontal growth of MoS_2 and WS_2* Nano Letters **14** 6842-6849

[24] J. Guo, X. Chen, Y. Yi, W. Li and C. Liang (2014) *Layer-controlled synthesis of graphene-like MoS_2 from single source organometallic precursor for Li-ion batteries* RSC Advances **4** 16716-16720

[25] Y.-H. Lee, *et al.* (2013) *Synthesis and transfer of single-layer transition metal disulfides on diverse surfaces* Nano Letters **13** 1852-1857

[26] D. Kong, H. Wang, J. J. Cha, M. Pasta, K. J. Koski, J. Yao and Y. Cui (2013) *Synthesis of MoS_2 and $MoSe_2$ films with vertically aligned layers* Nano Letters **13** 1341-1347

[27] A. L. Elías, *et al.* (2013) *Controlled synthesis and transfer of large-area WS_2 sheets: From single layer to few layers* ACS Nano **7** 5235-5242

[28] Y. M. Shi, *et al.* (2012) *Van der Waals epitaxy of MoS_2 layers using graphene as growth templates* Nano Letters **12** 2784-2791

[29] A. Castellanos-Gomez, M. Barkelid, A. M. Goossens, V. E. Calado, H. S. J. van der Zant and G. A. Steele (2012) *Laser-thinning of MoS_2: On demand generation of a single-layer semiconductor* Nano Letters **12** 3187-3192

[30] L. Hu, X. Shan, Y. Wu, J. Zhao and X. Lu (2017) *Laser thinning and patterning of MoS_2 with layer-by-layer precision* Scientific Reports **7** 15538

[31] S. Luo, S. Dong, C. Lu, C. Yu, Y. Ou, L. Luo, J. Sun and J. Sun (2018) *Rational and green synthesis of novel two-dimensional WS_2/MoS_2 heterojunction via direct exfoliation in ethanol-water targeting advanced visible-light-responsive photocatalytic performance* Journal of Colloid and Interface Science **513** 389-399

[32] H. Kaur, S. Yadav, A. K. Srivastava, N. Singh, S. Rath, J. J. Schneider, O. P. Sinha and R. Srivastava (2018) *High-yield synthesis and liquid-exfoliation of two-dimensional belt-like hafnium disulphide* Nano Research **11** 343-353

[33] H. Yu, H. Zhu, M. Dargusch and Y. Huang (2018) *A reliable and highly efficient exfoliation method for water-dispersible MoS_2 nanosheet* Journal of Colloid and Interface Science **514** 642-647

[34] J. N. Coleman, *et al.* (2011) *Two-dimensional nanosheets produced by liquid exfoliation of layered materials* Science **331** 568-571

[35] V. Nicolosi, M. Chhowalla, M. G. Kanatzidis, M. S. Strano and J. N. Coleman (2013) *Liquid exfoliation of layered materials* Science **340** 1226419

[36] Y.-M. Lin, *et al.* (2011) *Wafer-scale graphene integrated circuit* Science **332** 1294-1297

[37] S. Zhou, L. Gan, D. Wang, H. Li and T. Zhai (2017) *Space-confined vapor deposition synthesis of two dimensional materials* Nano Research DOI: https://doi.org/10.1007/s12274-017-1942-3.

[38] X. Song, Z. Guo, Q. Zhang, P. Zhou, W. Bao and D. W. Zhang (2017) *Progress of large-scale synthesis and electronic device application of two-dimensional transition metal dichalcogenides* Small **13** 1700098

[39] H. Li, H. Wu, S. Yuan and H. Qian (2016) *Synthesis and characterization of vertically standing MoS_2 nanosheets* Scientific Reports **6** 21171

[40] Y. Feng, *et al.* (2015) *Synthesis of large-area highly crystalline monolayer molybdenum disulfide with tunable grain size in a H_2 atmosphere* ACS Applied Materials & Interfaces **7** 22587-22593

[41] M. Ju, X. Liang, J. Liu, L. Zhou, Z. Liu, R. G. Mendes, M. H. Rümmeli and L. Fu (2017) *Universal substrate-trapping strategy to grow strictly monolayer transition metal dichalcogenides crystals* Chemistry of Materials **29** 6095-6103

[42] A. M. van der Zande, P. Y. Huang, D. A. Chenet, T. C. Berkelbach, Y. You, G.-H. Lee, T. F. Heinz, D. R. Reichman, D. A. Muller and J. C. Hone (2013) *Grains and grain boundaries in highly crystalline monolayer molybdenum disulphide* Nature Materials **12** 554-561

[43] Z. Lin, Y. Zhao, C. Zhou, R. Zhong, X. Wang, Y. H. Tsang and Y. Chai (2015) *Controllable growth of large–size crystalline MoS_2 and resist-free transfer assisted with a Cu thin film* Scientific Reports **5** 18596

[44] P. K. Mohapatra, S. Deb, B. P. Singh, P. Vasa and S. Dhar (2016) *Strictly monolayer large continuous MoS_2 films on diverse substrates and their luminescence properties* Applied Physics Letters **108** 042101

[45] Y. Yu, C. Li, Y. Liu, L. Su, Y. Zhang and L. Cao (2013) *Controlled scalable synthesis of uniform, high-quality monolayer and few-layer MoS_2 films* Scientific Reports **3** 1866

[46] S. Wang, Y. Rong, Y. Fan, M. Pacios, H. Bhaskaran, K. He and J. H. Warner (2014) *Shape evolution of monolayer MoS_2 crystals grown by chemical vapor deposition* Chemistry of Materials **26** 6371-6379

[47] D. M. Dobkin and M. K. Zuraw (2003) *Principles of Chemical Vapor Deposition* Dordrecht Springer Science+Business Media

[48] K.-K. Liu, *et al.* (2012) *Growth of large-area and highly crystalline MoS_2 thin layers on insulating substrates* Nano Letters **12** 1538-1544

[49] Y.-C. Lin, W. Zhang, J.-K. Huang, K.-K. Liu, Y.-H. Lee, C.-T. Liang, C.-W. Chu and L.-J. Li (2012) *Wafer-scale MoS_2 thin layers prepared by MoO_3 sulfurization* Nanoscale **4** 6637-6641

[50] Y. Zhan, Z. Liu, S. Najmaei, P. M. Ajayan and J. Lou (2012) *Large-area vapor-phase growth and characterization of MoS_2 atomic layers on a SiO_2 substrate* Small **8** 966-971

[51] A. Burzlaff, C. Beevers, H. Pearce, M. Lloyd and K. Klipsch (2017) *New studies on the in vitro genotoxicity of sodium molybdate and their impact on the overall assessment of the genotoxicity of molybdenum substances* Regulatory Toxicology and Pharmacology **86** 279-291

[52] Y. Tian, Y. He and Y. Zhu (2003) *Hydrothermal synthesis of fine Mos_2 crystals from Na_2MoO_4 and KSCN* Chemistry Letters **32** 768-769

[53] A. Michail, N. Delikoukos, J. Parthenios, C. Galiotis and K. Papagelis (2016) *Optical detection of strain and doping inhomogeneities in single layer MoS_2* Applied Physics Letters **108** 173102

[54] J. C. Meyer, C. Kisielowski, R. Erni, M. D. Rossell, M. F. Crommie and A. Zettl (2008) *Direct Imaging of Lattice Atoms and Topological Defects in Graphene Membranes* Nano Letters **8** 3582-3586

[55] B. Brox and I. Olefjord (1988) *ESCA Studies of MoO_2 and MoO_3* Surface and Interface Analysis **13** 3-6

[56] D. Ganta, S. Sinha and R. T. Haasch (2014) *2-D Material Molybdenum Disulfide Analyzed by XPS* Surface Science Spectra **21** 19-27

[57] S. Y. Yang, G. W. Shim, S.-B. Seo and S.-Y. Choi (2017) *Effective shape-controlled growth of monolayer MoS_2 flakes by powder-based chemical vapor deposition* Nano Research **10** 255-262

[58] J. Cheng, T. Jiang, Q. Ji, Y. Zhang, Z. Li, Y. Shan, Y. Zhang, X. Gong, W. Liu and S. Wu (2015) *Kinetic nature of grain boundary formation in as-grown MoS_2 monolayers* Advanced Materials **27** 4069-4074

[59] A. Govind Rajan, J. H. Warner, D. Blankschtein and M. S. Strano (2016) *Generalized mechanistic model for the chemical vapor deposition of 2D transition metal dichalcogenide monolayers* ACS Nano **10** 4330-4344

[60] T. Michely, M. Hohage, M. Bott and G. Comsa (1993) *Inversion of growth speed anisotropy in two dimensions* Physical Review Letters **70** 3943-3946

[61] J. D. Cain, F. Shi, J. Wu and V. P. Dravid (2016) *Growth mechanism of transition metal dichalcogenide monolayers: The role of self-seeding fullerene nuclei* ACS Nano **10** 5440-5445

[62] D. Dumcenco, *et al.* (2015) *Large-area epitaxial monolayer MoS_2* ACS Nano **9** 4611-4620

[63] C. Lee, H. Yan, L. E. Brus, T. F. Heinz, J. Hone and S. Ryu (2010) *Anomalous lattice vibrations of single- and few-layer MoS_2* ACS Nano **4** 2695-2700

[64] P. K. Chow, R. B. Jacobs-Gedrim, J. Gao, T.-M. Lu, B. Yu, H. Terrones and N. Koratkar (2015) *Defect-Induced Photoluminescence in Monolayer Semiconducting Transition Metal Dichalcogenides* ACS Nano **9** 1520-1527

[65] A. Castellanos-Gomez, R. Roldán, E. Cappelluti, M. Buscema, F. Guinea, H. S. J. van der Zant and G. A. Steele (2013) *Local strain engineering in atomically thin MoS_2* Nano Letters **13** 5361-5366

[66] H. J. Conley, B. Wang, J. I. Ziegler, R. F. Haglund, S. T. Pantelides and K. I. Bolotin (2013) *Bandgap engineering of strained monolayer and bilayer MoS_2* Nano Letters **13** 3626-3630

[67] P. Gerd, C.-G. Andres, B. Michele, S. J. v. d. Z. Herre, A. S. Gary, K. Agnieszka, H. Thomas, S. Christian and K. Tobias (2015) *Control of biaxial strain in single-layer molybdenite using local thermal expansion of the substrate* 2D Materials **2** 015006

[68] Y. L. Wang, C. X. Cong, C. Y. Qiu and T. Yu (2013) *Raman spectroscopy study of lattice vibration and crystallographic orientation of monolayer MoS_2 under uniaxial strain* Small **9** 2857-2861

[69] C. R. Zhu, *et al.* (2013) *Strain tuning of optical emission energy and polarization in monolayer and bilayer MoS_2* Physical Review B **88** 121301

[70] R. Yan, J. R. Simpson, S. Bertolazzi, J. Brivio, M. Watson, X. Wu, A. Kis, T. Luo, A. R. Hight Walker and H. G. Xing (2014) *Thermal conductivity of monolayer molybdenum disulfide obtained from temperature-dependent Raman spectroscopy* ACS Nano **8** 986-993

[71] B. Chakraborty, A. Bera, D. V. S. Muthu, S. Bhowmick, U. V. Waghmare and A. K. Sood (2012) *Symmetry-dependent phonon renormalization in monolayer MoS_2 transistor* Physical Review B **85**

[72] T. Jiang, H. Liu, D. Huang, S. Zhang, Y. Li, X. Gong, Y.-R. Shen, W.-T. Liu and S. Wu (2014) *Valley and band structure engineering of folded MoS_2 bilayers* Nature Nanotechnology **9** 825-829

[73] N. Bandaru, R. S. Kumar, D. Sneed, O. Tschauner, J. Baker, D. Antonio, S.-N. Luo, T. Hartmann, Y. Zhao and R. Venkat (2014) *Effect of pressure and temperature on structural stability of MoS_2* The Journal of Physical Chemistry C **118** 3230-3235

[74] K. F. Mak, C. Lee, J. Hone, J. Shan and T. F. Heinz (2010) *Atomically thin MoS_2: a new direct-gap semiconductor* Physical Review Letters **105** 136805

[75] K. F. Mak, K. He, C. Lee, G. H. Lee, J. Hone, T. F. Heinz and J. Shan (2013) *Tightly bound trions in monolayer MoS_2* Nature Materials **12** 207-211

[76] E. S. Kadantsev and P. Hawrylak (2012) *Electronic structure of a single MoS_2 monolayer* Solid State Communications **152** 909-913

[77] N. Scheuschner, O. Ochedowski, A.-M. Kaulitz, R. Gillen, M. Schleberger and J. Maultzsch (2014) *Photoluminescence of freestanding single- and few-layer MoS_2* Physical Review B **89** 125406

[78] A. Splendiani, L. Sun, Y. Zhang, T. Li, J. Kim, C.-Y. Chim, G. Galli and F. Wang (2010) *Emerging photoluminescence in monolayer MoS_2* Nano Letters **10** 1271-1275

[79] G. Anagnostopoulos, C. Androulidakis, E. N. Koukaras, G. Tsoukleri, I. Polyzos, J. Parthenios, K. Papagelis and C. Galiotis (2015) *Stress transfer mechanisms at the submicron level for graphene/polymer systems* Acs Applied Materials & Interfaces **7** 4216-4223

[80] M. S. Bronsgeest, N. Bendiab, S. Mathur, A. Kimouche, H. T. Johnson, J. Coraux and P. Pochet (2015) *Strain Relaxation in CVD Graphene: Wrinkling with Shear Lag* Nano Letters **15** 5098-5104

[81] Z. Li, I. A. Kinloch, R. J. Young, K. S. Novoselov, G. Anagnostopoulos, J. Parthenios, C. Galiotis, K. Papagelis, C. Y. Lu and L. Britnell (2015) *Deformation of wrinkled graphene* ACS Nano **9** 3917-3925

[82] Z. Liu, *et al.* (2014) *Strain and structure heterogeneity in MoS_2 atomic layers grown by chemical vapour deposition* Nature Communications **5** 5426

[83] S. Kataria, S. Wagner, T. Cusati, A. Fortunelli, G. Iannaccone, H. Pandey, G. Fiori and M. C. Lemme (2017) *Growth-Induced Strain in Chemical Vapor Deposited Monolayer MoS_2 : Experimental and Theoretical Investigation* Advanced Materials Interfaces **4** 1700031

[84] C. Rice, R. J. Young, R. Zan, U. Bangert, D. Wolverson, T. Georgiou, R. Jalil and K. S. Novoselov (2013) *Raman-scattering measurements and first-principles calculations of strain-induced phonon shifts in monolayer MoS_2* Physical Review B **87**

[85] D. Lloyd, X. Liu, J. W. Christopher, L. Cantley, A. Wadehra, B. L. Kim, B. B. Goldberg, A. K. Swan and J. S. Bunch (2016) *Band Gap Engineering with Ultralarge Biaxial Strains in Suspended Monolayer MoS_2* Nano Letters **16** 5836-5841

[86] E. Scalise, M. Houssa, G. Pourtois, V. V. Afanas′ev and A. Stesmans (2014) *First-principles study of strained 2D MoS_2* Physica E: Low-dimensional Systems and Nanostructures **56** 416-421

[87] E. Scalise, M. Houssa, G. Pourtois, V. Afanas'ev and A. Stesmans (2012) *Strain-induced semiconductor to metal transition in the two-dimensional honeycomb structure of MoS_2* Nano Research **5** 43-48